JOURNAL OF SOLID STATE CHEMISTRY 71, 331–341 (1987)

Nonstoichiometry and Structural Intergrowth in the $CaFe_xMn_{1-x}O_{3-y}$ ($0 \leq x \leq 1$) System

JOSÉ M. GONZÁLEZ-CALBET, JOSÉ ALONSO, AND MARÍA VALLET-REGÍ

Departamento de Química Inorgánica, Facultad de Química, Universidad Complutense, 28040 Madrid, Spain

Received November 26, 1986; in revised form February 3, 1987

An electron diffraction and microscopy study of the $CaFe_xMn_{1-x}O_{3-y}$ system treated at 1100°C in air has been performed. An increase of y is accompanied by an increase of the cubic perovskite substructure parameter, the nonstoichiometry being accommodated in several ways. The system contains two solid solutions of the perovskite-type (P) and of the brownmillerite-type (B) and also an intermediate phase ($x = 0.6$) which makes disordered intergrowth with the B-type solid solution. These results are discussed in terms of multitwinning, randomly dispersed oxygen deficiency, and ordered and disordered intergrowth formation.

Introduction

In recent years, a considerable amount of work has dealt with nonstoichiometry in AMO_{3-x} perovskites since compositional variations can lead in some circumstances to the formation of new materials. In order to produce defects in the anionic sublattice of the perovskite-type structure (*1*) two conditions seem to be necessary: (i) The elements occupying the *M* positions have to be able to adopt several coordinations, and (ii) a situation of mixed oxidation states in either *A* or *M* cations is necessary so that the formation of anionic vacancies can be possible.

Iron (*2–4*), titanium (*5*), cobalt (*6, 7*), manganese (*8–10*), copper (*11–14*), and nickel (*15*), among others, have led to the formation of various phases in the AMO_3–$AMO_{2.5}$ composition range with perovskite-related structures. However, it seems that the situation becomes more complicated when two of these cations share the *M* position. Thus, several studies have been performed in the $CaFe_xMn_{1-x}O_{3-y}$ system. Depending on the temperature, oxygen pressure, and oxide precursors, iron and manganese can adopt various oxidation states and then, several polyhedral environments, leading to different ways to accommodate the nonstoichiometry (*16–21*).

In order to clarify the information concerning this system, we have performed a study of electron diffraction and microscopy of two series of samples of the title system having different compositions and prepared them at 1100 and 1400°C in air, respectively. We have previously reported (*22*) that samples heated at 1400°C in air accommodate the nonstoichiometry by means of the intergrowth of $Ca_2Fe_2O_5$-like domains and/or $CaMnO_3$-like domains in the region $0.2 \leq x \leq 0.4$. In this paper, we

0022-4596/87 $3.00

report work in the $CaMnO_3$–$Ca_2Fe_2O_5$ composition range of the samples prepared at 1100°C.

Experimental

Samples of various compositions of the $CaFe_xMn_{1-x}O_{3-y}$ system were prepared from stoichiometric mixtures of $CaCO_3$, $MnCO_3$, and α-Fe_2O_3. An intimate mixture of the reagents was preheated in air at 1000°C for 45 hr to decompose the carbonate. After that treatment, samples were fired in air at 1400°C for 45 hr and then annealed at 1100°C for 4 days and quenched to room temperature. The black materials thus obtained were homogeneous under the optical microscope.

Powder X-ray characterization was performed on a Siemens D-500 diffractometer using Cu$K\alpha$ radiation and silicon as the internal standard.

The average oxidation state of iron in the samples was determined by chemical analysis with H_3PO_4 solution after dilution in HCl 1 : 1 with an excess of Mohr's salt. The amounts of both Mn^{4+} and Mn^{3+} were determined as previously described (*22*). Total amounts of manganese and iron were confirmed by atomic absorption spectrometry.

Electron diffraction and microscopy were performed on a Philips EM 400T electron microscope fitted with a double-tilting goniometer stage, by working at 120 kV, kindly lent to us by the Laboratoire de Cristallographie, CNRS, Grenoble, France. The samples were ultrasonically dispersed in *n*-butanol and then transferred to carbon-coated copper grids.

Results

Powder X-ray diffraction patterns of all the studied samples show diffraction maxima corresponding either to the perovskite structure or to some superlattices of such a structural type. However, only some of these patterns can be characterized as single phases, the other corresponding, at a first sight, to phase mixtures. Table I summarizes the unit cell parameters of the various samples and their composition as deduced from the chemical analysis.

Single Phases

x = 0.2 sample. $CaFe^{4+}_{0.2}Mn^{4+}_{0.60}Mn^{3+}_{0.20}O_{2.90}$ gave a powder X-ray diffraction pattern similar to that obtained for $CaMnO_3$ (P), which can be indexed on the basis of a tetragonal cell with parameters related to the cubic perovskite subcell by $a_c\sqrt{2} \times 2a_c \times a_c\sqrt{2}$, where $a_c = 3.746$ Å is the pseudocu-

TABLE I

CHEMICAL ANALYSIS DATA AND UNIT CELL PARAMETERS OF THE DIFFERENT SAMPLES

x	Chemical composition	Structural type	a (Å)	b (Å)	c (Å)	a_c (Å)
0	$CaMn^{4+}O_3$	$CaMnO_3$ (*23*)	5.279(1)	7.448(1)	5.264(1)	3.726
0.2	$CaFe^{4+}_{0.2}Mn^{4+}_{0.60}Mn^{3+}_{0.20}O_{2.90}$	$CaMnO_3$(P)	5.297(2)	7.495(3)	5.297(2)	3.746
0.3	$CaFe^{4+}_{0.3}Mn^{4+}_{0.39}Mn^{3+}_{0.31}O_{2.845}$	Cubic perovskite	3.755(2)	—	—	3.755
0.4	$CaFe^{4+}_{0.22}Fe^{3+}_{0.18}Mn^{4+}_{0.35}Mn^{3+}_{0.25}O_{2.785}$	$CaMnO_3$ + $A_3M_3O_8$	—	—	—	—
0.5	$CaFe^{3+}_{0.5}Mn^{4+}_{0.40}Mn^{3+}_{0.10}O_{2.70}$	$CaMnO_3$ + $A_3M_3O_8$	—	—	—	—
0.6	$CaFe^{3+}_{0.6}Mn^{4+}_{0.37}Mn^{3+}_{0.03}O_{2.685}$	$A_3M_3O_8$ (G)	5.476(1)	11.151(3)	5.360(1)	3.793
0.7	$CaFe^{3+}_{0.7}Mn^{4+}_{0.24}Mn^{3+}_{0.06}O_{2.62}$	$A_3M_3O_8$ + brownmillerite	—	—	—	—
0.8	$CaFe^{3+}_{0.8}Mn^{4+}_{0.11}Mn^{3+}_{0.09}O_{2.555}$	$A_3M_3O_8$ + brownmillerite	—	—	—	—
0.9	$CaFe^{3+}_{0.9}Mn^{4+}_{0.09}Mn^{3+}_{0.01}O_{2.545}$	Brownmillerite (B)	5.563(1)	14.835(5)	5.409(1)	3.822
1	$Ca_2Fe^{3+}_2O_5$	Brownmillerite (*24*)	5.5980(5)	14.7687(17)	5.4253(5)	3.829

bic unit cell parameter. However, Poeppelmeier *et al.* (*23*) have shown by a single-crystal X-ray study that $CaMnO_3$ is orthorhombic with $a = 5.279$ Å, $b = 7.448$ Å, and $c = 5.264$ Å, where $a_c = 3.726$ Å, but such a small orthorhombic distortion cannot be detected by the conventional powder diffractometers.

As can be seen, chemical analysis reveals a certain amount of oxygen deficiency, $y = 0.10$. Electron microscopy is the most suitable technique to investigate the way in which these anionic vacancies are accommodated. Figure 1 shows the electron diffraction pattern and the corresponding electron micrograph of this sample along the [001] zone axis of the perovskite substructure. This micrograph and some electron diffraction patterns obtained by tilting around either a^* or b^* indicate that this material is formed by three sets of twinned domains of $CaMnO_3$ type with the double axis alternating at random in the three space directions. Three-dimensional multitwinning has been already observed in slightly distorted orthorhombic perovskites such as $LaFeO_3$ (*25*) and $SrSnO_3$ (*26*). Moreover, the $x = 0.2$ sample of this system treated at 1400°C also showed this situation (*22*). In regard to the composition of this high-temperature sample, i.e., $Ca Fe^{3+}_{0.20}Mn^{3+}_{0.35}Mn^{4+}_{0.45}O_{2.72}$, it seems that in the presence of manganese the iron stabilizes as Fe^{3+} better than as Fe^{4+} at high temperature, leading to higher amounts of anionic vacancies. In order to check whether nonstoichiometry is responsible for the twinning, the end member of this system, $CaMnO_3$, was studied by electron diffraction and microscopy. Such study shows an electron diffraction pattern analogous to that observed in the above sample, the elec-

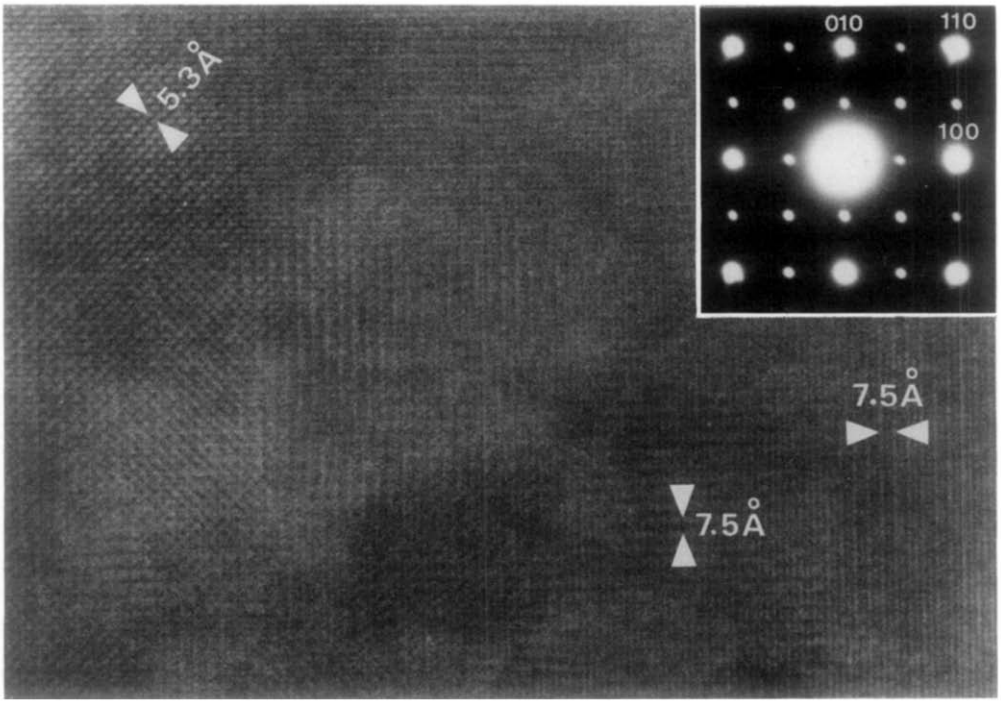

FIG. 1. Electron micrograph of the $x = 0.2$ sample along the $[001]_c$ zone axis and a selected electron diffraction pattern (inset). Several domains with the perovskite doubled axis oriented at random in one of the three space directions are seen.

tron micrograph showing domains of larger size. It seems, then, that anionic vacancies are disordered at random in the crystal, preserving the perovskite symmetry.

$x = 0.3$ sample. Chemical analysis of this sample reveals an increase of the percentage of Mn(III) while iron remains as Fe(IV), the oxygen deficiency being $y = 0.15$. On the other hand, all the maxima appearing in the powder X-ray diffraction pattern can be indexed on the basis of a simple cubic perovskite cell of parameter $a_c = 3.755(1)$ Å. The electron diffraction patterns of all the crystals studied corresponding to this material show neither superstructure spots nor streaking of the diffraction maxima. Only the basic reflections corresponding to the cubic perovskite cell were observed. Moreover, electron microscopy only reveals the ~3.8 Å lattice fringes of the (100) d spacings of the perovskite.

This lack of superstructure spots indicates that the anionic vacancies are either dispersed at random in the crystal, giving an average cubic symmetry characteristic of long-distance disorder of such vacancies, or if some kind of ordering exists, it would be nonperiodic and its contribution to the diffraction patterns would appear in the incoherent background between Bragg reflections. At this point, it is to be noted that Komornicki *et al.* (*27*) hypothesized, based on theoretical calculations, that the vacancy ordering varies continually as a function of y. For values of y close to 0.15, as in this case, oxygen vacancies were thought to be ordered along rows of various lengths in a statistical fashion, preserving the cubic perovskite symmetry.

$x = 0.6$ sample. As deduced from the chemical analysis, the amount of iron in this system increases with the increasing percentage of Fe^{3+}, Fe^{4+} not being found in this sample. By X-ray diffraction this solid was found to be orthorhombic with unit cell parameters related to the a_c parameter of the cubic perovskite by $a_c\sqrt{2} \times 3a_c \times a_c\sqrt{2}$. Figure 2 shows the electron diffraction pattern and the corresponding micrograph of this material along the [001] zone axis. A threefold superlattice of the perovskite structure along the b axis is observed, characteristic of the $A_3M_3O_8$-type structure (*28*), in which two octahedral layers alternate with one tetrahedral layer along this axis. This kind of solid has been already found in the $CaFe_xMn_{1-x}O_{3-y}$ system by Hervieu *et al.* (*21*) in the $0.53 \leq x \leq 0.57$ composition range. A study by X-ray diffraction and Mössbauer spectroscopy by these authors (*20*) shows that the structure of the $x = 0.55$ solid presents some differences with respect to the structural model described for the $n = 3$ member of the $A_nM_nO_{3n-1}$ series (*29*). Additional oxygen atoms were observed in the tetrahedral layers with an occupancy factor $\tau = 0.3$ instead of 0, whereas the octahedral layers were found to exhibit an oxygen defect corresponding to an occupancy factor $\tau = 0.7$ instead of 1 for the ideal structure. This was explained by the ability of Mn^{3+} to adopt square pyramidal coordination.

Chemical analysis indicates that our sample has $Ca_3Fe^{3+}_{1.8}Mn^{4+}_{1.11}Mn^{3+}_{0.09}O_{8.055}$ composition and, in spite of the oxygen excess ($\delta = 0.055$) with respect to the ideal $A_3M_3O_8$ structure (G), no disorder is seen in either electron diffraction patterns or micrographs. Since Mn^{4+} certainly prefers to remain in an octahedral environment and Fe^{3+} can adopt both octahedral and tetrahedral configurations, the small quantity of Mn^{3+} having pyramidal surroundings is distributed at random along the crystal, meaning that $Ca_3(Fe_xMn_{3-x})O_{8\pm\delta}$ shows nonstoichiometry at least in the $1.60 \leq x \leq 1.80$ range, with δ varying from -0.012 to $+0.055$.

$x = 0.9$ sample. According to the X-ray diffraction pattern, the $x = 0.9$ solid is orthorhombic, with unit cell parameters $a_c\sqrt{2} \times 4a_c \times a_c\sqrt{2}$ corresponding to a

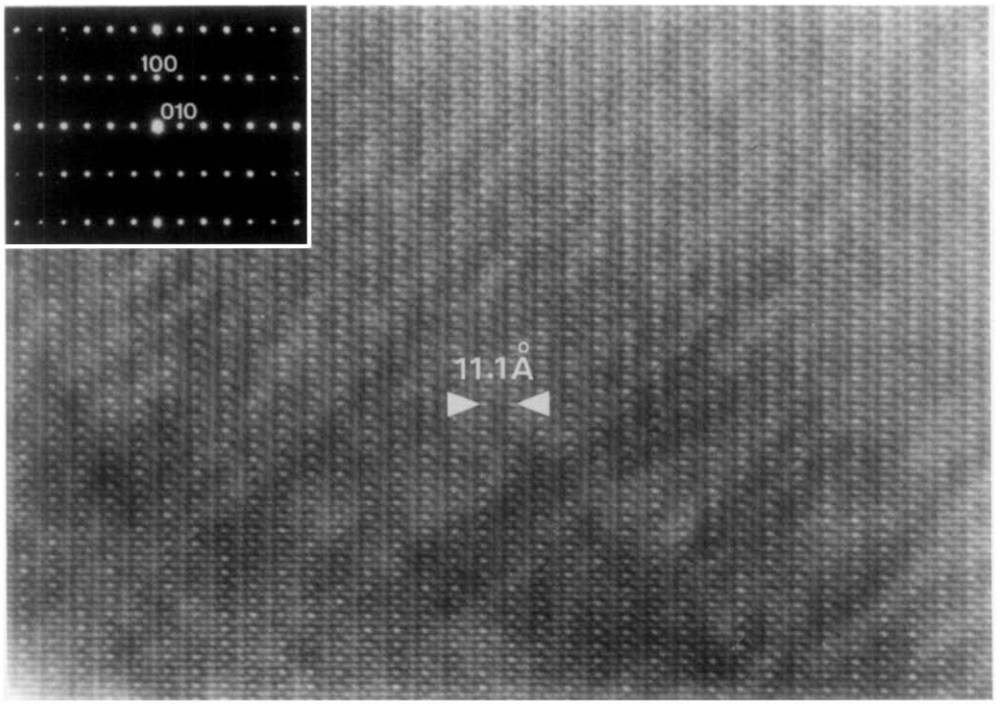

FIG. 2. The electron diffraction pattern along the $[001]_G$ zone axis and the corresponding micrograph of the $x = 0.6$ sample, showing an interplanar spacing of 11.1 Å characteristic of the stacking sequence $\cdots OOT \cdots$.

brownmillerite-type structure (B) (*30*). The composition as deduced from the chemical analysis is $Ca_2Fe^{3+}_{1.8}Mn^{4+}_{0.18}Mn^{3+}_{0.02}O_{5.09}$. Once again, the electron diffraction pattern and the corresponding electron micrograph (Fig. 3) show an ordered material with the characteristic diffraction maxima and *d* spacings of a brownmillerite-type structure of $A_2M_2O_5$ composition (B). Since no extra spots were observed in the electron microscopy study, the oxygen excess must be randomly distributed, a brownmillerite-type solid solution being obtained in the $0.9 \leq x \leq 1$ composition range of the $CaFe_xMn_{1-x}O_{3-y}$ system.

Phase Mixtures

$0.4 \leq x \leq 0.5$ samples. These samples showed very complex powder X-ray diffraction patterns but all of the reflections of both $x = 0.4$ and $x = 0.5$ solids could be indexed on the basis of a phase mixture of both P- and G-type structures. The complexity of these patterns is due to the existence of two superstructures of the same structural type, leading to the overlapping of many of the diffraction maxima. Thus, although the intensity of the lines corresponding to $CaMnO_3$ was very small in the $x = 0.5$ sample, they were clearly appreciable.

An electron microscopy study of the $Ca_xLa_{1-x}FeO_{3-x/2}$ system in the $0.2 \leq x \leq 0.66$ range (*25*) showed that samples giving similar X-ray diffraction patterns accommodated the nonstoichiometry by means of disordered intergrowth between $LaFeO_3$ and $Ca_2LaFe_3O_8$. However, such a study in the $CaFe_xMn_{1-x}O_{3-y}$ system confirms the existence of two types of crystals, with P and G structures, respectively.

$0.7 \leq x \leq 0.8$ samples. Once again, the

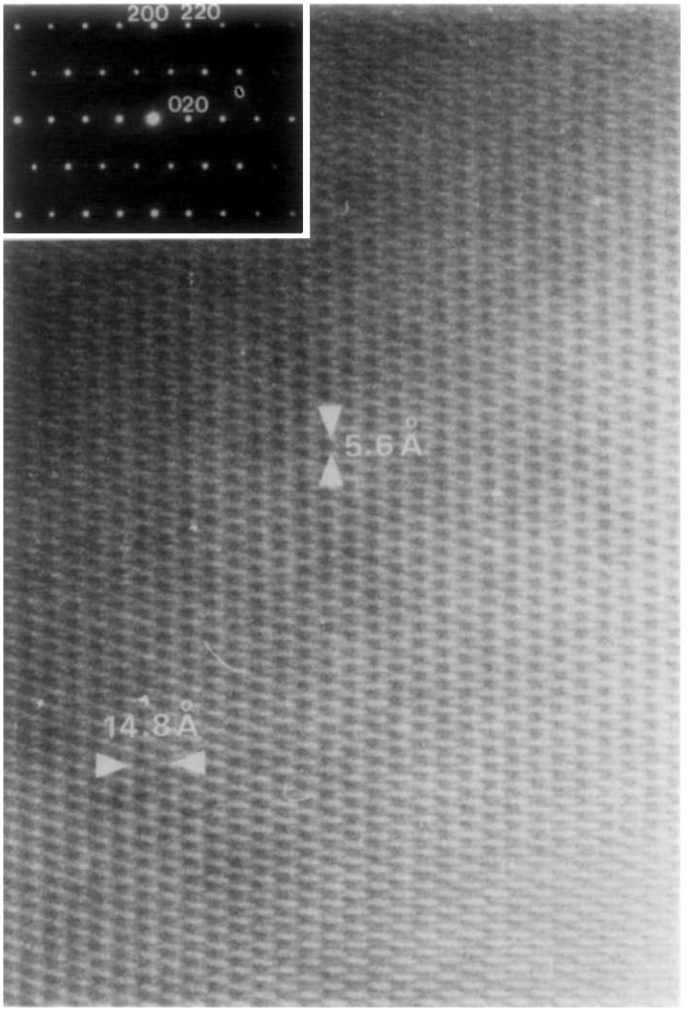

FIG. 3. An electron micrograph of the $x = 0.9$ sample, showing the $d_{010} = 14.8$ Å and $d_{100} = 5.6$ Å spacings of the brownmillerite-type structure. No disorder is seen along the crystal. Inset: A selected electron diffraction pattern along $[001]_B$.

X-ray diffraction data of the samples were interpreted as due to a phase mixture, but now of both G- and B-type structures. However, the electron diffraction and microscopy show a more complex real situation. Figure 4a shows the electron diffraction pattern of the $x = 0.7$ sample along the $[10\bar{1}]_c$ zone axis of the cubic perovskite substructure. In addition to the strong reflections corresponding to the perovskite structure, two different kinds of diffraction maxima can be seen in this pattern:

(i) A series of spots corresponding to the $[001]_G$ zone axis of an $A_3M_3O_8$-type structure ($a_c\sqrt{2} \times 3a_c \times a_c\sqrt{2}$) schematically shown in Fig. 4b.

(ii) Another set of maxima which can be indexed in the $[001]_B$ zone axis of the brownmillerite unit cell ($a_c\sqrt{2} \times 4a_c \times a_c\sqrt{2}$), schematically shown in Fig. 4c.

The corresponding electron micrograph (Fig. 4d) shows that these crystals are formed by a disordered intergrowth be-

tween regions characterized by a spacing of 14.8 Å = d_{010} of the brownmillerite-type structure and other regions in which the spacing is 11.1 Å, i.e., d_{010} of the G phase. From these results and comparing the line intensities in the X-ray diffraction pattern, we can determine, although not quantitatively, that for the $X = 0.7$ composition, the amount of brownmillerite phase is slightly larger than that of $A_3M_3O_8$. However, for $x = 0.8$, although the same disordered intergrowths are observed, the brownmillerite phase is by far the most abundant.

Discussion

Since X-ray diffraction only detects long-range periodicity, electron diffraction and lattice imaging are necessary to follow the clustering of anionic vacancies when the oxygen deficiency increases from the perovskite (P)- to the brownmillerite (B)-type structures. Figure 5 summarizes a tentative phase diagram for the $CaFe_xMn_{1-x}O_{3-y}$ system at 1100°C as deduced from the above electron microscopy study. It can be seen that only an ordered intermediate phase exists between the perovskite and the brownmillerite, for $x = 0.6$, which can be described as an ordered intergrowth between a half brownmillerite unit cell (OT) and one perovskite unit cell (O) following the stacking sequence $\cdots$OOTOOT$\cdots$ (O = octahedron, T = tetrahedron). This structural model was initially proposed by Grenier *et al.* (*31*) for $Ca_3Fe_2TiO_8$ where all Ti^{4+} are octahedrally coordinated while Fe^{3+} remains in both octahedral and tetrahedral coordination.

As mentioned above, $Ca_3(Fe_xMn_{3-x})O_{8\pm\delta}$ ($1.6 < x < 1.8$) allows nonstoichiometry due to the presence of Mn(III) in square pyramidal coordination. Thus, it seems that the G structural type stabilizes when the oxygen content per unit formula y is around 0.33, which can be attained either with the stacking sequence $\cdots$OOTOOT$\cdots$ along all the crystal or by substituting one octahedron and one tetrahedron by two square pyramids. Obviously, such a substitution must be limited to a restricted number of crystallographic sites, since this phase is only stable for a few x values. According to Nguyen *et al.* (*20*), if only Mn^{3+} shows pyramidal coordination, there will be very few sites showing such a coordination in the $x = 0.6$ sample, being very close to an "ideal" G phase.

In order to obtain such ordered sequence we prepared a sample with $x = 0.66$ composition. However, according to the chemical analysis, some Mn^{3+} is still present as reflected in the formula $CaFe^{3+}_{0.66}Mn^{4+}_{0.31}Mn^{3+}_{0.02}O_{2.64}$, the oxygen deficiency being large enough to allow, as observed by electron microscopy, the presence of fringes of 14.8 Å, corresponding to the brownmillerite-type structure dipersed within the G-type structure.

As it is well known, the structure and the homogeneity range of a compound is closely related with its history, i.e., it depends of the reagents and treatment conditions. Thus, some small differences are observed in the homogeneity range between our samples and those prepared by Nguyen *et al.* (*20*) since precursor oxides and annealing times are different. However, Rao *et al.* (*32*) by decomposing carbonate solid solutions at 1000°C and reducing the resulting oxide in dilute hydrogen at 330°C, obtained the $Ca_3Fe_2MnO_{7.5}$ oxide. Under these conditions, the anionic deficiency is larger than in $Ca_3Fe_2MnO_8$; since all of the manganese is in the 3+ oxidation state, the most probable structure of the oxide is one involving a stacking sequence $\cdots$POTPOT$\cdots$ (P = square pyramid) along the b axis.

No more anion-vacancy-ordered superstructures have been found in this system between the perovskite and the brownmillerite structures. However, as studied by X-ray diffraction and electron microscopy, we can detect in the $CaFe_xMn_{1-x}O_{3-y}$ system three types of solid solutions showing

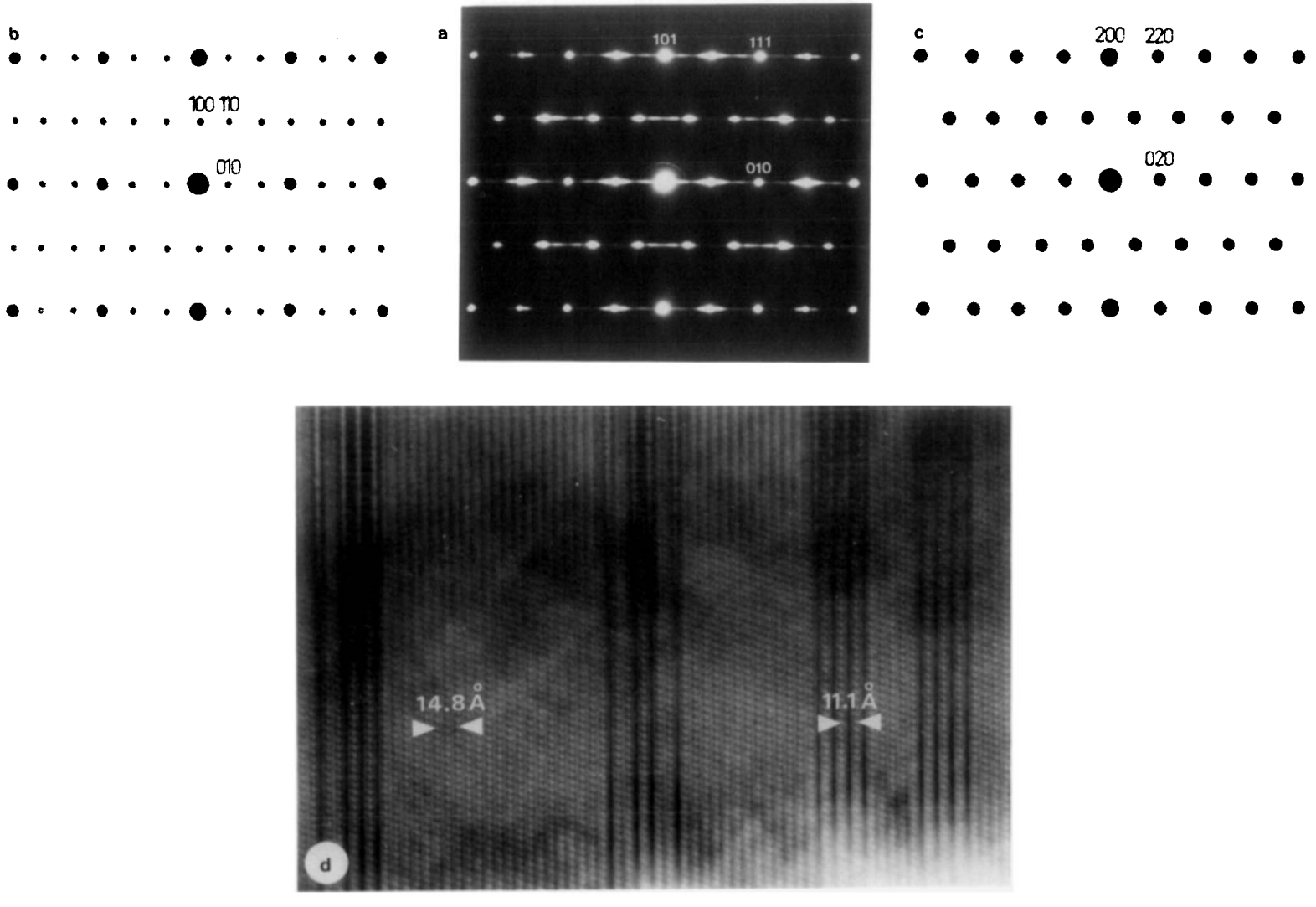
b
100 110
010
a
101
111
010
c
200 220
020
14.8 Å
11.1 Å
d

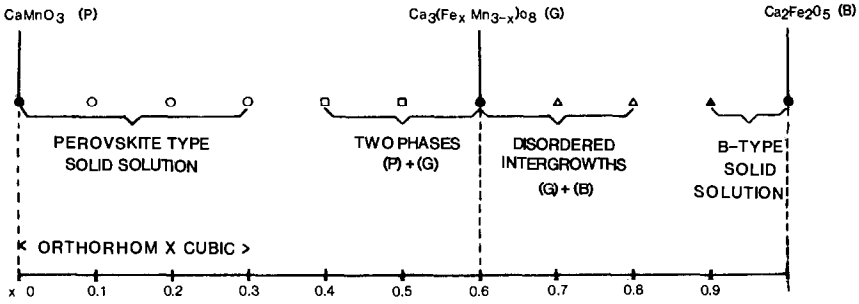

FIG. 5. A schematic phase diagram of the $CaFe_xMn_{1-x}O_{3-y}$ system at 1100°C.

nonstoichiometry where, obviously, anionic vacancies are randomly dispersed: (i) A perovskite-type solid solution in the $0 < x \leq 0.3$ composition range, (ii) the $Ca_3(Fe_xMn_{3-x})O_{8\pm\delta}$ solid solution already mentioned, and (iii) a brownmillerite-type solid solution for $0.9 \leq x < 1$. Comparing the three perovskite substructures we see that the a_c parameter (Fig. 6) increases with increasing iron content, following a Vegard's rule (*33*). This may be attributed to the larger ionic size of Fe^{3+} (octahedral and tetrahedral coordination), Fe^{4+} (octahedral coordination), and Mn^3 (square pyramidal coordination) with respect to Mn^{4+} (octahedrally coordinated) and also due to the logical increase in the anionic vacancies which produces a less compact structure. Since the cation substitution in the three solid solutions is accompanied by a change in the oxidation state, the solid solutions can be considered examples of anomalous solid solutions.

The last way of accommodation of the nonstoichiometry observed in this system is by the formation of disordered intergrowths between two different structural types. It can be observed in Table I that the three phases coexisting in this system, P, G, and B, have two similar parameters, the *b* axis being different. This situation can lead to the intergrowth between such phases, as has already been found in other perovskite-related systems (*25, 34*), where the information obtained by means of X-ray diffraction studies is insufficient to detect this phenomenon. Electron microscopy has allowed us to elucidate that in the $CaFe_xMn_{1-x}O_{3-y}$ system, the intergrowth is only possible between the G and B phases, but not in the composition range between the perovskite and the G phases, where a mixture of both kind of crystals is observed. Regarding the parameters of the three phases, that *a* and *c* of G and B phases are more similar than those corresponding to P and G phases can be appreciated. For this reason, the structural distortion required for the intergrowth of G and P along the *b* axis would be too great, such accommodation of nonstoichiometry being much more energetically favorable when the values of *a* and *c* are closer. In this way, the $Ca_xLa_{1-x}FeO_{3-y}$ system (*25*) is formed by the disordered intergrowth of two out of three ordered terms:

	$a \simeq a_c\sqrt{2}$	$b \simeq na_c$	$c \simeq a_c\sqrt{2}$
$LaFeO_3$	5.563 Å	7.867 Å	5.553 Å
$Ca_2LaFe_3O_8$	5.563 Å	11.29 Å	5.467 Å
$Ca_2Fe_2O_5$	5.598 Å	14.7687 Å	5.4253 Å

FIG. 4. (a) An electron diffraction pattern of the $x = 0.7$ sample along $[10\bar{1}]_c$ equivalent to $[001]_G$ (b) and to $[001]_B$ (c). (d) An electron micrograph corresponding to the pattern shown in a. Disordered intergrowth between the G (d_{010} = 11.1 Å) and B (d_{010} = 14.8 Å) phases are clearly seen.

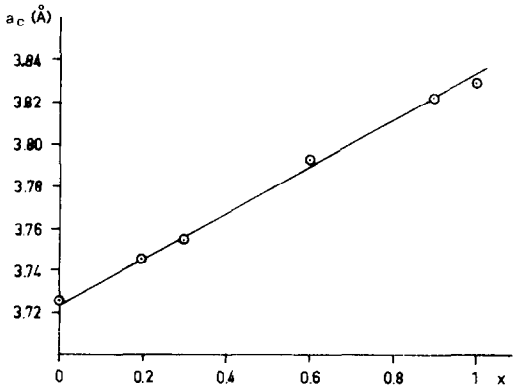

FIG. 6. Evolution of the pseudocubic parameter a_c as a function of iron content.

It can be observed that the a and c parameters are very similar. In these circumstances, the distortion necessary for the coupling of two phases is small, intergrowth being favorable. When the perovskite phase is $CaMnO_3$, the differences with the G parameters are more pronounced, single phases of both resultant structural types being more stable.

From the results obtained, it is evident, once again, that the major problem that occurs in the investigation of long-range order in oxides arises from the fact that the material is often in a metastable condition and, then, poorly equilibrated phases are the rule rather than the exception in ceramic oxide materials.

Acknowledgments

We thank M. Perroux (Laboratoire de Cristallographie, CNRS, Grenoble) and A. García (Instituto "Elhúyar," CSIC, Madrid) for technical assistance and the CAICYT (Spain) for financial support.

References

1. H. D. Megaw, "Crystal Structures: A Working Approach." Sanders, London (1973).
2. B. C. TOFIELD, C. GREAVES, AND B. E. F. FENDER, *Mater. Res. Bull.* **10,** 737 (1975).
3. J. C. GRENIER, M. POUCHARD, AND P. HAGENMULLER, *Struct. Bonding* **47,** 1 (1981).
4. Y. TAKEDA, K. KANNO, T. TAKADA, O. YAMAMOTO, M. TAKANO, N. NAKAYAMA, AND Y. BANDO, *J. Solid State Chem.* **63,** 237 (1986).
5. M. A. ALARIO-FRANCO AND M. VALLET-REGÍ, *Nature (London)* **270,** 706 (1977).
6. J. C. GRENIER, S. GHODBANE, G. DEMAZEAU, M. POUCHARD, AND P. HAGENMULLER, *Mater. Res. Bull.* **14,** 831 (1979).
7. J. RODRÍGUEZ AND J. M. GONZÁLEZ-CALBET, *Mater. Res. Bull.* **21,** 429 (1986).
8. A. RELLER, D. A. JEFFERSON, J. M. THOMAS, R. A. BEYERTEIN, AND K. R. POEPPELMEIER, *J. Chem. Soc. Chem. Commun.*, p. 1378 (1982).
9. A. RELLER, D. A. JEFFERSON, J. M. THOMAS, AND M. K. UPPAL, *J. Phys. Chem.* **87,** 913 (1983).
10. A. RELLER, J. M. THOMAS, D. A. JEFFERSON AND M. K. UPPAL, *Proc. R. Soc. London A* **394,** 223 (1984).
11. V. CAIGNAERT, M. HERVIEU, N. NGUYEN, AND B. RAVEAU, *J. Solid State Chem.* **62,** 281 (1986).
12. N. NGUYEN, L. ER-RAKHO, C. MICHEL, J. CHOISNET, AND B. RAVEAU, *Mater. Res. Bull.* **15,** 891 (1980).
13. J. PROVOST, F. STUDER, C. MICHEL, AND B. RAVEAU, *Synth. Met.* **4,** 147 (1981).
14. N. NGUYEN, J. CHOISNET, M. HERVIEU, AND B. RAVEAU, *J. Solid State Chem.* **39,** 120 (1981).
15. K. VIDYASAGAR, A. RELLER, J. GOPALAKRISHNAN, AND C. N. R. RAO, *J. Chem. Soc., Chem. Commun.*, p. 7 (1985).
16. R. V. COATES AND J. W. MCMILLAN, *J. Appl. Chem.* **14,** 346 (1964).
17. E. BANKS, D. BERKOOZ, AND T. NAKAGAWA, *NBS (U.S.) Spec. Publ.* **364,** 265 (1972).
18. T. AKIYAMA, *Mater. Res. Bull.* **16,** 469 (1981).
19. T. AKIYAMA, *Mater. Res. Bull.* **16,** 1074 (1981).
20. N. NGUYEN, Y. CALOGE, F. VARRET, G. FEREY, V. CAIGNAERT, M. HERVIEU, AND B. RAVEAU, *J. Solid State Chem.* **53,** 398 (1984).
21. M. HERVIEU, N. NGUYEN, V. CAIGNAERT, AND B. RAVEAU, *Phys. Status Solidi A* **83,** 473 (1984).
22. M. VALLET-REGÍ, J. M. GONZÁLEZ-CALBET, J. VERDE, AND M. A. ALARIO-FRANCO, *J. Solid State Chem.* **57,** 197 (1985).
23. K. R. POEPPELMEIER, M. E. LEONOWICZ, AND J. M. LONGO, *J. Solid State Chem.* **44,** 89 (1982).
24. J. BERGGREN, *Acta Chem. Scand.* **25,** 3616 (1971).
25. M. VALLET-REGÍ, J. GONZÁLEZ-CALBET, M. A. ALARIO-FRANCO, J. C. GRENIER, AND P. HAGENMULLER, *J. Solid State Chem.* **55,** 251 (1984).
26. A. VEGAS, M. VALLET-REGÍ, J. M. GONZÁLEZ-CALBET, AND M. A. ALARIO-FRANCO, *Acta Crystallogr. B* **42,** 167 (1986).
27. S. KOMORNICKI, J. C. GRENIER, M. POUCHARD,

AND P. HAGENMULLER, *Nuovo J. Chim.* **5,** 161 (1981).

28. J. C. GRENIER, F. MENIL, M. POUCHARD, AND P. HAGENMULLER, *Mater. Res. Bull.* **12,** 79 (1977).
29. J. C. GRENIER, G. SCHIFFMACHER, P. CARO, M. POUCHARD, AND P. HAGENMULLER, *J. Solid State Chem.* **20,** 365 (1977).
30. E. F. BERTAUT, P. BLUM, AND A. SAGNIERES, *Acta Crystallogr.* **12,** 149 (1959).
31. J. C. GRENIER, J. DARRIET, M. POUCHARD, AND P. HAGENMULLER, *Mater. Res. Bull.* **11,** 1219 (1976).
32. C. N. R. RAO, J. GOPALAKRISHNAN, K. VIDYASAGAR, A. K. GANGULI, A. RAMANAN, AND L. GANAPATHI, *J. Mater. Res.* **1,** 280 (1986).
33. L. VEGARD, *Z. Phys.* **5,** 393 (1921).
34. J. M. GONZÁLEZ-CALBET, M. VALLET-REGÍ, M. A. ALARIO-FRANCO, AND J. C. GRENIER, *Mater. Res. Bull.* **18,** 285 (1983).